

# Chaos-assisted free-space coupling and transmission spectra of high-Q deformed microcavities

Qi-Fan Yang,<sup>\*</sup> Xue-Feng Jiang, Ya-Long Cui, Linbo Shao, Yun-Feng Xiao,<sup>†</sup> and Qihuang Gong<sup>‡</sup>  
*State Key Lab for Mesoscopic Physics, Department of Physics, Peking University, P. R. China*

We investigate the mechanism of efficient excitation of high-Q modes in deformed microcavities via the chaos-assisted free-space coupling. A quantum scattering theory is employed to study the free-space transmission properties, from which the coupling strength can be derived. The theory predicts asymmetric Fano-like resonances around high-Q modes in background transmission spectra, which is in good agreement with previous experimental results. The phase shift occurring in the dynamical tunneling across Kolmogorov-Arnol'd-Moser tori is further studied, which plays a key role in the Fano-like resonance. This efficient free-space coupling holds potential advantages in simplifying experimental condition and exciting high-Q modes in higher-index-material microcavities.

## I. INTRODUCTION

Over last two decades, optical whispering-gallery-mode (WGM) microresonators (or microcavities) [1] with high quality factors and small mode volumes have promised lab-on-chip applications ranging from fundamental physics to various photonic devices, such as nonlinear optics [2–4], cavity quantum electrodynamics [5, 6], cavity optomechanics [7–9], optical communications [10, 11], low-threshold microlasing [12–15] and highly sensitive optical biosensing [16–21]. In these applications, traditionally light is coupled into the WGM microcavities by evanescent couplers, such as prisms [22], tapered fibers [23, 24] and angle-polished fibers [25], which have been validated to be highly efficient. In all of these coupling configurations, the microcavity is typically separated from the coupler by a distance of subwavelength because the evanescent field of WGMs extends over a very short range. The use of the evanescent couplers, however, is not suitable in some important applications. For example, a higher-index-material microcavity [4] can not be efficiently excited by the tapered fiber due to phase mismatching. In addition, the external couplers degrade the high-Q property in the case of the over-coupling regime, and they are not convenient in low-temperature chambers.

It has been demonstrated that WGMs in a specially designed deformed cavity can be directly excited by a free-space optical beam [8, 26, 27]. This direct free-space coupling is of importance because it is robust and requires less rigorous experimental condition than the evanescent couplers mentioned above. The efficient free-space coupling originates from the breaking of rotational symmetry in deformed microcavities, which produces a highly directional emission assisted by the dynamical tunneling, different from the isotropic nature of a circular WGM cavity [26–28]. According to the time reversion, *i.e.*, the reversibility of light path, free-space beams at certain positions are expected to couple into the high-Q modes via chaos when they are on resonance. So far, this type of free-space coupling technique has been demonstrated experi-

mentally to reach a resonant efficiency exceeding 50% [29]. A straightforward method to characterize the free-space coupling is to study its transmission property, *e.g.*, transmission spectrum. In this paper, we investigate the dynamical tunneling properties between the chaos and the regular modes in detail, and predict transmission spectra of the free-space coupling by employing a quantum scattering theory. It is found that the spectrum can behave asymmetrically as Fano-like lineshape [30], in good agreement with our recent experimental observation [31]. With the theoretical model, the coupling strength to the regular high-Q mode can be further derived from the transmission spectrum.

This paper is organized as follows. In Sec. II, we present the mechanism of chaos-assisted free-space coupling, and introduce a quantum scattering theory to predict a general transmission. It is found that the transmission spectrum includes the contribution from both the off-resonance background and the on-resonance modulation. In Sec. III, we study the off-resonance background transmission in the absence of the high-Q regular mode, from which the unperturbed scattering is characterized. In Sec. IV, the on-resonance transmission spectra are studied in detail. They depend strongly on (i) the additional phase when light travels in chaotic trajectories and (ii) the rate of dynamical tunneling. Sec. V further investigates the phase shift occurring in the dynamical tunneling process, which plays a key role in obtaining Fano-resonance lineshapes in the transmission spectra.

## II. CHAOS-ASSISTED FREE-SPACE COUPLING

Before studying the transmission spectrum, we briefly address the mechanism of the chaos-assisted free-space coupling. Poincaré surface of section (PSOS) provides a simple and intuitive way to model the ray dynamics in deformed microcavities, similar to billiards in quantum chaos. Except for an integrable ellipse-shaped cavity, the deformed microcavity has a mixed phase space including three types of structures: Kolmogorov-Arnol'd-Moser (KAM) tori, islands, and chaotic sea, corresponding to quasi-periodicity, periodicity, and chaotic motion of ray trajectories. High-Q modes are usually localized in the regular regions [32, 33], *e.g.*, the KAM tori which can be described by a perturbed Hamiltonian [34]. For such a localized high-Q mode, the excitation by free-space

<sup>\*</sup>Electronic address: leonardoyoung@pku.edu.cn

<sup>†</sup>Author to whom correspondence should be addressed: yfxiao@pku.edu.cn;  
 URL: [www.phy.pku.edu.cn/~yfxiao/index.html](http://www.phy.pku.edu.cn/~yfxiao/index.html)

<sup>‡</sup>Electronic address: qhgong@pku.edu.cn

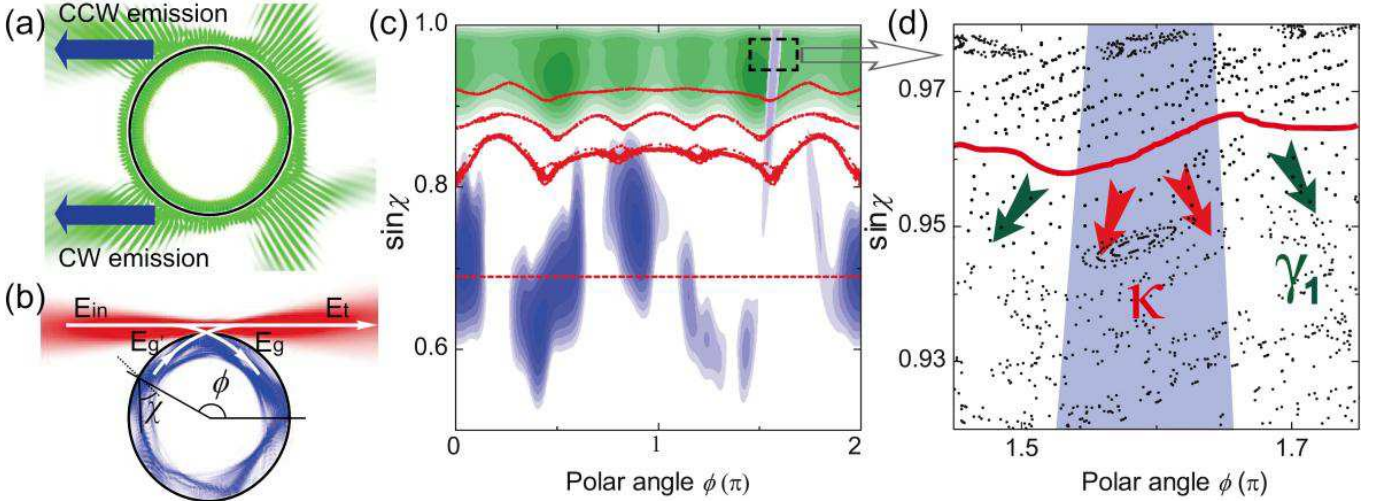


FIG. 1: (Color online) (a) False color illustration of a resonant mode distribution obtained with wave simulation. The two blue arrows denote the unidirectional emission toward  $180^\circ$  far-field direction. The strength outside the cavity is magnified for clear show. (b) Schematic illustration of a deformed microcavity excited by a free-space laser beam. The polar angle  $\phi$  and the incident angle of rays  $\chi$  give the coordinates of Poincaré surface of section. (c) Husimi projection of the excitation state (blue) and resonant state (green) in log scale, corresponding to (a) and (b), respectively. The red dashed curve represents the critical line determined by  $\sin \chi = 1/n$ . The red dotted curves above  $\sin \chi = 0.8$  stand for some typical KAM tori which divides the phase space into discontinuing regions. (d) Enlarged view of the area of the dashed rectangle in (c). Red solid line denotes a regular mode, and black dots indicates the chaotic sea. Red arrows represent the coupling to the chaos with strength  $\kappa$ , and green arrows stand for the decay into other chaotic states which contributes to the loss  $\gamma_1$  in Eq. 4.

beam is primarily attributed to two channels: (i) *angular momentum tunneling* and (ii) *dynamical tunneling via chaos* [35]. It has been demonstrated that the dynamical tunneling dominates, since the lifetime of photons that refract into the deformed cavity greatly increases along chaotic trajectories [26].

Without loss of generality, here we consider a two-dimensional deformed cavity made of silica with refractive index  $n = 1.45$ , which has the boundary defined in polar coordinates as

$$R(\phi) = \begin{cases} R_0(1 + \eta \sum_{i=2,3} a_i \cos^i \phi), & \text{for } \cos \phi \geq 0 \\ R_0(1 + \eta \sum_{i=2,3} b_i \cos^i \phi), & \text{for } \cos \phi < 0 \end{cases} \quad (1)$$

where  $R_0$  and  $\eta$  represent size and deformation parameters, respectively. Cavity shape parameters are set as  $a_2 = -0.1329$ ,  $a_3 = 0.0948$ ,  $b_2 = -0.0642$ ,  $b_3 = -0.0224$ . When  $\eta = 1$ , a highly unidirectional far-field universal pattern of high-Q modes has been predicted [36] and demonstrated experimentally [37]. This emission characteristic is clearer by plotting the near-field pattern, as shown in Fig. 1(a). It can be seen that there exist two major emission positions at  $\phi = \pi/2, 3\pi/2$ , corresponding to refractive escape from counter-clockwise (CCW) and clockwise (CW) modes, respectively. Thus, we expect with a time reversed way, an excitation beam focused on the primary emission position at  $\phi = \pi/2$  shown in Fig. 1(b), can eventually excite the CW resonant modes. To quantitatively study this chaos-assisted process, we now use a quantum scattering theory to model the transmission spectrum, from which the coupling characteristic

of the high-Q mode can be obtained.

In the system consisting of a microcavity and unbounded medium outside, the state  $|\psi_\omega\rangle$  which describes the electromagnetic field excited by the incident beam satisfies stationary Schrödinger equation

$$H |\psi_\omega\rangle = \omega |\psi_\omega\rangle, \quad (2)$$

where  $H$  stands for the system Hamiltonian. As mentioned above, not only chaos but the regular mode can also be excited by an appropriate free-space beam thanks to the dynamical tunneling. This can be demonstrated by plotting the Husimi projection [38] of the excitation state  $|\psi_\omega\rangle$ , as shown in Fig. 1(c). Thus  $|\psi_\omega\rangle$  can be expanded as a linear combination of chaos  $|C_\omega\rangle$  and regularity  $|WGM\rangle$  [39], with the form

$$|\psi_\omega\rangle = a_\omega |WGM\rangle + \int d\omega' b_\omega(\omega') |C_{\omega'}\rangle. \quad (3)$$

The system Hamiltonian satisfies

$$\langle WGM | H | WGM \rangle = \omega_0 - i\gamma/2, \quad (4a)$$

$$\langle C_{\omega'} | H | C_{\omega'} \rangle = \omega\delta(\omega' - \omega), \quad (4b)$$

$$\langle C_\omega | H | WGM \rangle = V_\omega. \quad (4c)$$

Here  $\omega_0$  and  $\omega$  are the frequencies of the resonant regular mode and the incident light, respectively. The coupling coefficient between  $|C_\omega\rangle$  and  $|WGM\rangle$ , governed by the dynamical tunneling, is described by  $V_\omega$ . The decay rate  $\gamma$  consists of the intrinsic loss and the chaos-assisted tunneling loss. In detail, the intrinsic decay rate  $\gamma_0$  is attributed to radiation,

material absorption and scattering losses in the cavity, while the chaos-assisted decay rate  $\gamma_1$  describes tunneling into the chaotic states other than  $|C_\omega\rangle$ .

In this paper, we consider the chaotic states as continuum and use a standard quantum scattering model to interpret the transmission lineshape. Here we assume that  $|C_\omega\rangle$  and  $|WGM\rangle$  are orthogonal [40]. Substituting Eq. 3 into Eq. 2, the coefficients  $a$  and  $b$  are determined by

$$(\omega_0 - i\gamma/2)a_\omega + \int d\omega' V_\omega^* b_\omega(\omega') = \omega a_\omega, \quad (5a)$$

$$V_\omega a_\omega + \omega' b_\omega(\omega') = \omega b_\omega(\omega'). \quad (5b)$$

On the one hand, applying a standard treatment [30], the coefficient  $b$  yields

$$b_\omega(\omega') = \left[ \frac{1}{\omega - \omega'} + z_\omega \delta(\omega - \omega') \right] V_\omega a_\omega, \quad (6)$$

where

$$z_\omega = \frac{\omega - \omega_0 + i\gamma/2 - F(\omega)}{|V_\omega|^2}. \quad (7)$$

The shift of resonant frequency is expressed as  $F(\omega) = \text{v.p.} \int \kappa / (2\pi(\omega - \omega')) d\omega'$  where v.p. denotes Cauchy's principle value. The reduced coupling strength  $\kappa$  between  $|C_\omega\rangle$  and  $|WGM\rangle$  is obtained through the Fermi's golden rule under the first Markov approximation [41], with

$$\kappa = 2\pi |V_\omega|^2. \quad (8)$$

For high-Q mode in slightly deformed cavity whose intrinsic line width  $\gamma$  is orders of magnitude smaller than the resonant frequency  $\omega_0$ , the bounds of the integral of  $F(\omega)$  can be extended to infinity, resulting in

$$F(\omega) = \frac{\kappa}{2\pi} \text{v.p.} \int_{-\infty}^{+\infty} d\omega' \frac{1}{\omega - \omega'} = 0. \quad (9)$$

On the other hand, the normalization condition  $\langle \psi_\omega | \psi_\omega \rangle = \delta(\omega' - \omega)$  determines the value of  $a$  by

$$|a_\omega|^2 |V_\omega|^2 [\pi^2 + |z_\omega|^2] \delta(\omega' - \omega) + a_\omega^* a_\omega \frac{i\gamma_0}{\omega' - \omega} = \delta(\omega' - \omega). \quad (10)$$

By integrating this equation over  $\omega$ , we have

$$|a_\omega|^2 = \frac{1}{2\pi} \frac{\kappa}{(\omega - \omega_0)^2 + (\frac{\gamma + \kappa}{2})^2}. \quad (11)$$

In Eq. 11,  $|a_\omega|^2$  describes the excitation probability by the free-space beam, from which we can deduce that the FWHM (full width at half maximum) of the regular mode is expressed as  $\kappa + \gamma \equiv \gamma_t$ . The decay rate  $\gamma_t$  can be measured directly from the free-space transmission spectra. It should be noted that  $\gamma_t$  remains unchanged when the free-space coupling efficiency changes [27], which is distinguished with the fiber taper coupling.

Finally, the transmission spectrum is calculated as

$$\begin{aligned} T(\omega) &= |\langle \psi_\omega | S | \text{in} \rangle|^2 \\ &= |a_\omega|^2 |\langle WGM + \text{v.p.} \int d\omega' \frac{V_\omega}{\omega - \omega'} C_{\omega'} \rangle|^2 \\ &\quad + \frac{(\omega - \omega_0 + i\gamma/2)V_\omega}{|V_\omega|^2} C_\omega |S | \text{in} \rangle|^2, \end{aligned} \quad (12)$$

where  $S$  is a suitable transmission operator connecting  $|\text{in}\rangle$  and  $|C_\omega\rangle$ , and  $|\langle C_\omega | S | \text{in} \rangle|^2$  describes the probability of transmitted signal [30]. To get a more general expression, we introduce a dimensionless frequency detuning defined by  $\epsilon \equiv (\omega - \omega_0)/(\kappa/2)$  and the ratio  $K \equiv \gamma/\kappa = (\gamma_t - \kappa)/\kappa$ . Therefore, the transmission is simplified to

$$T(\omega) = \frac{|q_\omega + \epsilon - iK|^2}{(1 + K)^2 + \epsilon^2} |\langle C_\omega | S | \text{in} \rangle|^2. \quad (13)$$

Here  $q_\omega$  represents the crucial lineshape parameter of the transmission spectrum  $T(\omega)$ , taking the form

$$q_\omega = \frac{\langle \varphi_\omega | S | \text{in} \rangle}{\pi V_\omega^* \langle C_\omega | S | \text{in} \rangle}, \quad (14)$$

where  $|\varphi_\omega\rangle = |WGM\rangle + \text{v.p.} \int d\omega' \frac{V_\omega |C_{\omega'}\rangle}{\omega - \omega'}$ . To give a clear understanding, we consider two extreme cases.

(i) In classical mechanics where the dynamical tunneling is forbidden, the regular mode cannot be excited. Thus there is no interaction between regular mode and the chaotic states ( $\kappa \rightarrow 0$ ), and the coefficients  $\epsilon, K \propto 1/\kappa$  as well as  $q_\omega \propto 1/\sqrt{\kappa}$ . In this case the transmission spectra yields to

$$T_0(\omega) = |\langle C_\omega | S | \text{in} \rangle|, \quad (15)$$

which can be regarded as the unperturbed scattering. In Sec. III we will discuss the unperturbed scattering, which is of much concerning about the lineshape near resonance.

(ii) When the intrinsic loss of regular mode is negligible and the regular mode is fully excited by a phase conjugation wave of its emission pattern, *i.e.*,  $\gamma \ll \kappa$  and  $K \rightarrow 0$ , the transmission yields a standard Fano resonance

$$T(\omega) = \frac{|q_\omega + \epsilon|^2}{1 + \epsilon^2} |\langle C_\omega | S | \text{in} \rangle|^2. \quad (16)$$

### III. OFF-RESONANCE TRANSMISSION

Before detailing the transmission spectrum around a high-Q regular mode, we investigate the background scattering in the absence of the regular mode. It has been reported that non-resonant pumping in deformed microcavity can be well modeled by ray dynamics [42, 43]. In our case, the unperturbed transmission is approximately determined by the interference between two components, according to the schema shown in Fig. 1(b): (i) the direct transmitted amplitude  $t$ , and (ii) the dissipated amplitude  $r$  via diffusing inside the cavity. To give

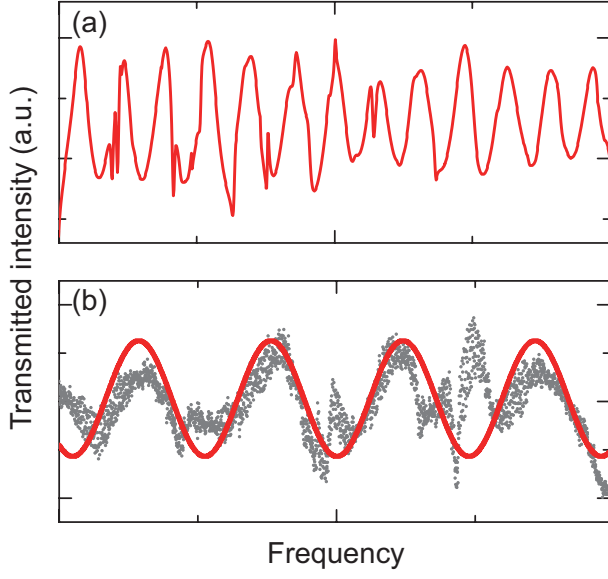


FIG. 2: (Color online) (a) Simulated transmission spectra via boundary element method. (b) Transmission spectra measured experimentally (grey dots) and fitting background oscillation corresponding to Eq. 20 (red solid line). These two graphs are plotted in different scales.

a clear picture of the interference, we apply transmission matrix, and the amplitudes on the interface are indicated by

$$\begin{pmatrix} E_t \\ E_g \end{pmatrix} = \begin{pmatrix} t & g' \\ g & t' \end{pmatrix} \begin{pmatrix} E_{in} \\ E_{g'} \end{pmatrix}. \quad (17)$$

$E_{g'}$  and  $E_g$  are related by

$$E_{g'} = \alpha E_g, \quad (18)$$

where  $\alpha$  is a coefficient including the loss and the phase change in a round trip. The transition matrix element is given by

$$\langle C_\omega | S | in \rangle = \frac{E_t}{E_{in}} = t + \frac{\alpha g' g}{1 - \alpha t'} = t + r e^{i\theta}. \quad (19)$$

Here  $r$  and  $\theta$  can be understood as the equivalent amplitude and phase shift of forward-emitted field from the cavity, respectively. Hence, the unperturbed transmission takes the form

$$T_0 = |\langle C_\omega | S | in \rangle|^2 = r^2 \left( 1 + \left(\frac{t}{r}\right)^2 + 2\frac{t}{r} \cos \theta \right). \quad (20)$$

In a wide frequency width  $\theta$  can be simplified as  $nkL_{\text{eff}}$  with  $L_{\text{eff}}$  representing the equivalent chaotic path length of the light inside the cavity. Thus the transmission spectrum shows periodic modulations in good agreement with numerically simulated transmission, as shown in Fig. 2(a). In experiment, we focus the incident beam on the periphery of a deformed microtoroid with the principle radius  $45\mu\text{m}$ , and the

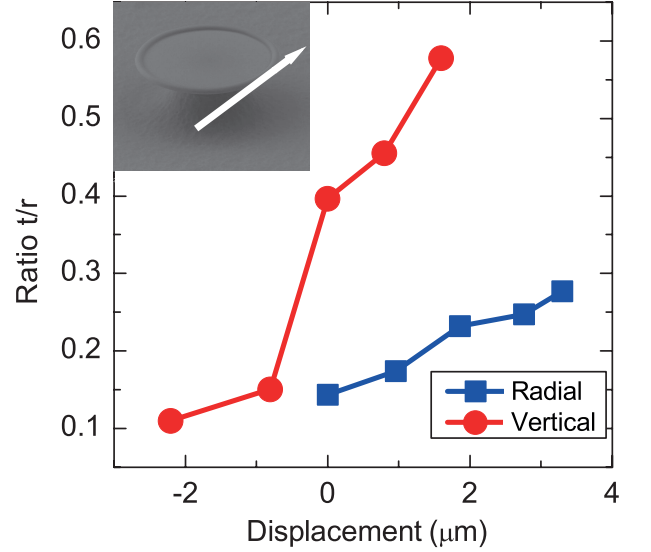


FIG. 3: (Color online) Experimental ratio of the amplitudes of the transmitting and refracting channels  $t/r$  depending on tuning the displacement in radial (red round spots) and vertical (blue square spots) direction. Inset: SEM image of the deformed microtoroid in oblique view. The white arrow represents the incident beam.

waist of the beam is about  $3\mu\text{m}$  [37]. Fig. 2(b) reveals that the experimentally detected transmission also oscillates periodically. The fitted ratio  $t/r$  for experiments increases with moving the focused spot away from the cavity in radial direction or lifting the beam in the vertical direction, and the latter response is more sensitive, as shown in Fig. 3. It is because the silicon substrate of the device blocks a portion of the incident light, asymmetrically in vertical direction. Thus, the focused spot changing vertically results in a remarkable impact on the direct transmitted amplitude.

#### IV. ON-RESONANCE TRANSMISSION

We now turn to the on-resonance transmission. It is noted that the direct excitation probability of high-Q regular modes via evanescent field is negligible due to angular momentum mismatch, so that the amplitude of  $\langle \text{WGM} | S | in \rangle$  in Eq. 14 has minor contribution of the transmission. In this case, the lineshape parameter  $q$  can be reduced to a simplified form. Substituting Eq. 19 into Eq. 14, we obtain the expression of the lineshape parameter

$$q_\omega = \frac{\text{v.p.} \int d\omega' \frac{1}{\omega - \omega'} V_{\omega'}^* \langle C_{\omega'} | S | in \rangle}{\pi V_\omega^* \langle C_\omega | S | in \rangle} = -\frac{ie^{i\theta}}{t/r + e^{i\theta}}, \quad (21)$$

where  $\theta = nkL_{\text{eff}}$  as mentioned above. Substituting Eq. 21 into Eq. 13, the on-resonance transmission can be deduced. In the following, we will show that the lineshape of the transmission spectrum is determined by  $q_\omega$ , which primarily depends on  $\theta$ , while the modulation depth relies on the relative coupling strength described by  $K$ .

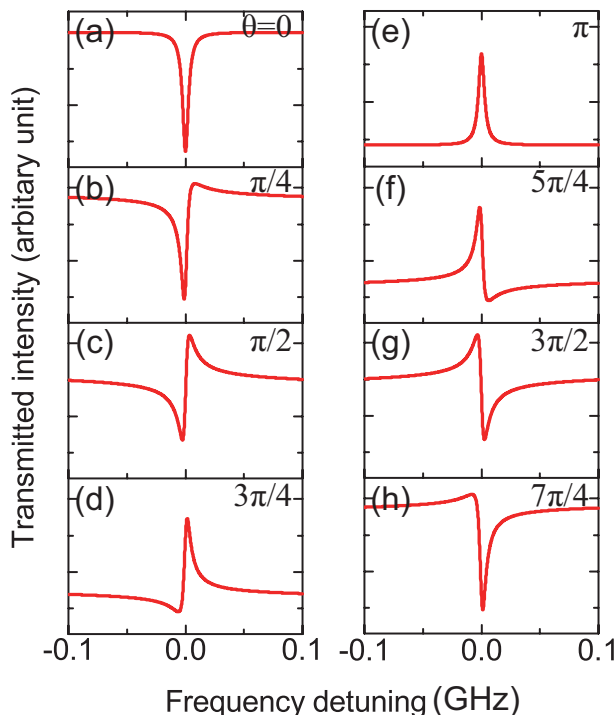


FIG. 4: (a)-(h) Calculated transmission spectra with  $\kappa/2\pi, \gamma/2\pi = 0.003$  GHz and  $t/r = 0.2$ . The phase shift between the two amplitudes varies from 0 to  $7\pi/4$ .

Figures 4(a)-4(h) plot calculated transmission spectra against  $\theta$ , which experience symmetric Lorentz absorption dips, asymmetric Fano-like lineshapes and symmetric electromagnetically-induced-transparency (EIT)-like peaks as  $\theta$  varies from 0 to  $2\pi$ . From Fig. 1(b), the transmission is a result of interference between two components: the direct transmitted light and the emitted light from the cavity, and  $\theta$  actually describes the phase difference between them. Interestingly, the on-resonance transmission appears a symmetric dip on the background where the two components constructively interfere ( $\theta = 0$  in Fig. 4(a)), while it switches to an EIT-like peak when they destructively interfere ( $\theta = \pi$  in Fig. 4(e)). This is because when on resonance, the chaos refractively excited by the incident beam can couple to the regular mode via dynamical tunneling, which results in a phase shift as energy couples back to the chaos. This phase shift in the round trip is semiquantitatively demonstrated  $\pi$  in Sec. V. Hence, although the background components constructively (destructively) interfere, such counteraction adds a destructive modulation to the chaos, reflecting a dip (peak) on the transmission.

As discussed above, the Fano-resonance transmission spectra can be regarded as the modulation of the high-Q mode on the off-resonance background. Such modulation depends strongly on the coupling strength  $\kappa$  between the chaos and the regular mode according to Eq. 13. Here we study the two special cases: EIT-like lineshapes and Lorentz dips. As shown in the solid curve in Fig. 5(a), the modulation of the regular mode to the transmission spectrum is minor when  $K = 60$ .

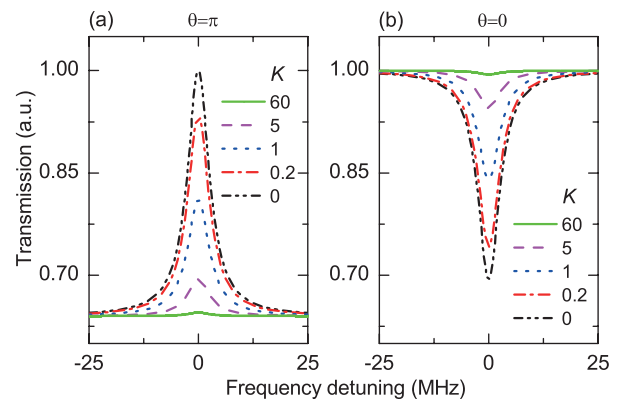


FIG. 5: (Color online) Calculated transmission spectra with  $\gamma_t/2\pi = 0.006$  GHz and  $t/r = 0.2$ , and with  $K$  varying from 0 to 60, for (a) EIT-like lineshape and (b) Lorentz-like lineshape. The background is set to the same level for each graph.

In this case, the excitation probability is extremely low. As  $K$  decreases (*i.e.*, the dynamical tunneling is enhanced), the height of the EIT peak increases monotonically, where the off-resonance backgrounds are lifted to the same level. When the intrinsic loss described by  $\gamma_0 + \gamma_1$  is negligible compared with the coupling strength  $\kappa$ , *i.e.*,  $K \rightarrow 0$ , the EIT peak reaches its maximum. Similarly, Fig. 5(b) shows that the dynamical-tunneling-induced dips become more obvious by enhancing the tunneling, as expected.

## V. PHASE SHIFT IN DYNAMICAL TUNNELING THROUGH KAM BARRIERS

Finally, we discuss the phase shift occurring in the dynamical tunneling through KAM curves [44, 45]. This phase shift is crucial to give rise to the Fano resonance. As shown in Fig. 1(c), KAM tori separate the phase space into disconnected regions, between which transport is forbidden classically, but permitted in quantum mechanics [46, 47], known as the dynamical tunneling. It is found that chaos contributes to the enhanced coupling strength. As shown in Figs. 6(a)-6(c), the Husimi projections of the excitation states inside the cavities depend on the deformation of the cavities. For  $\eta = 0$ , the KAM tori which fill the PSOS greatly prohibit the excitation of high-Q modes. As the deformation parameter increases, regular high-Q modes are more likely to be excited. To evaluate the tunneling effect, we study the case that a photon crosses an additional barrier to a regular periodic. For the sake of analytical expressions but without loss of the physics, we investigate the KAM barriers in the circular microcavity. The wave function of a WGM with angular momentum number  $m$  in circular cavities takes the form

$$\Psi(\mathbf{r}, \phi) = f_m(\mathbf{r})e^{im\phi} \quad (22)$$

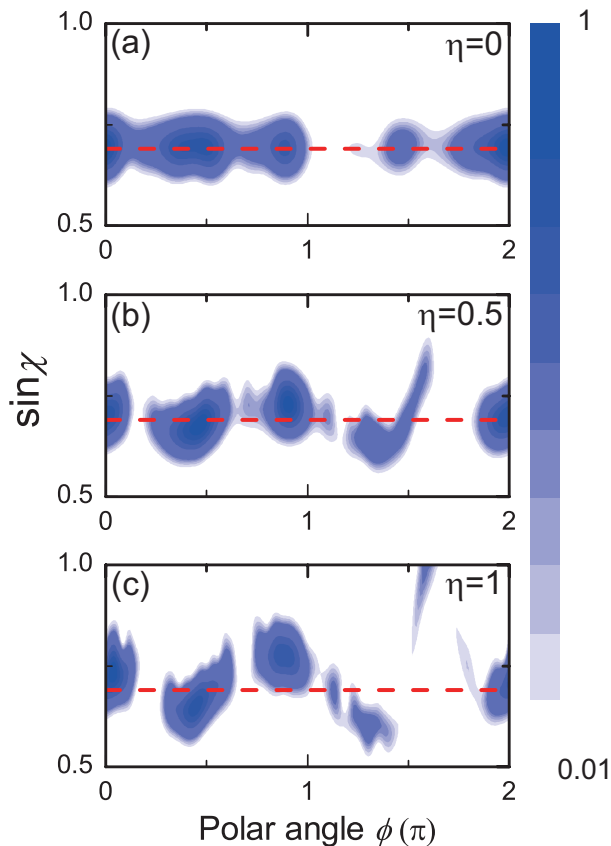


FIG. 6: (Color online) (a)-(c) Husimi projections of the excitation state inside the cavity at non-resonant frequency with deformation parameter  $\eta$  of the cavity set as [0, 0.5, 1] from top to bottom. The red dashed line denotes the critical line.

where  $f_m(\mathbf{r})$  satisfies the radial wave equation

$$\left[-\nabla_{\mathbf{r}}^2 - \frac{(n^2(\mathbf{r}) - 1)\omega^2}{c^2} + \frac{m^2}{r^2}\right]f_m(\mathbf{r}) = \frac{\omega^2}{c^2}f_m(\mathbf{r}). \quad (23)$$

Analogized to the stationary Schrödinger equation

$$\left(-\frac{\hbar^2}{2\mu}\nabla^2 + V\right)f_m(\mathbf{r}) = Ef_m(\mathbf{r}) \quad (24)$$

and substituted with  $E = \hbar\omega$ , we deduce the effective potential corresponding to the angular momentum number  $m$

$$V = \frac{\hbar^2}{2\mu} \left[ -\frac{(n(\mathbf{r})^2 - 1)\omega^2}{c^2} + \frac{m^2}{r^2} \right]. \quad (25)$$

Extending  $m$  to the range of positive real numbers, from the classical relation  $m = \pi/(\pi - 2\chi)$ , the potential takes the form

$$V(\sin \chi) = \frac{\hbar^2}{2\mu} \frac{\pi^2}{(\pi - 2\chi)^2 r_0^2} - c.c., \quad (26)$$

where  $r_0$  is the radius of the cavity. The effective potential  $V$  aggrandizes rapidly as  $\chi$  increases, and tends to infinity as  $\chi \sim \pi/2$ . The tunneling coefficient across this barrier is

$$t_p = \frac{1}{1 + i\mu V/\hbar^2 k}. \quad (27)$$

For the high-Q regular modes lying above  $\sin \chi > 0.95$ , the effective potential  $V$  is extremely large, so that  $\arg(t_p) \sim -\pi/2$ . Hence, a  $\pi$  phase shift emerges in the counteractive process  $|C_\omega\rangle \rightarrow |WGM\rangle \rightarrow |C_\omega\rangle$ , which leads to the transparency of chaos, as discussed in Sec. IV.

## VI. SUMMARY

In conclusion, we have presented the chaos-assisted mechanism to interpret how a free-space laser beam excites the high-Q modes in deformed microcavities. The deformed microcavity has a mixed phase space, where the high-Q regular modes lie in regular regions. Lifetime of photons refracting into the cavity increases due to chaotic trajectories, which contributes to the enhanced excitation of regular modes via *chaos-assisted dynamical tunneling*. A quantum scattering theory is employed to describe the picture and to obtain the free-space transmission. Unlike evanescent coupling with a waveguide where the transmission spectra behave symmetrically, this model predicts three types of transmission, *i.e.*, asymmetric Fano-like, symmetric EIT-like and Lorentz dip lineshapes, depending on the phase difference related to the fluctuation of background transmission. It is found that the Fano resonance is attributed to the phase shift occurring in the dynamical tunneling into classical-forbidden regions. Our results provide a general method to evaluate the coupling strength between the chaos and the regular mode from the transmission spectra, which can be further extended to the quantitative study of the dynamical tunneling process. The efficient chaos-assisted free-space coupling is of importance to simplifying experimental condition and exciting high-Q modes in higher-index-material microcavities.

## Acknowledgments

This work was supported by NSFC (Nos. 11004003, 11121091, and 11023003), 973 program (No. 2013CB328704), and RFDPH (No. 20090001120004). Q.F.Y. and Y.L.C. were supported by the National Fund for Fostering Talents of Basic Science (No. J1030310 and No. J1103205), and the Undergraduate Research Fund of Education Foundation of Peking University. Q.F.Y. and X.F.J. thank Prof. Fang-Jie Shu for discussions.

- 
- [1] *Optical Microcavities*, edited by K. Vahala (World Scientific, Singapore, 2005).
- [2] S.-X. Qian and R. K. Chang, *Phys. Rev. Lett.* **56**, 926 (1986).
- [3] S. M. Spillane, T. J. Kippenberg, and K. J. Vahala, *Nature* **415**, 623 (2002).
- [4] V. S. Ilchenko, A. A. Savchenkov, A. B. Matsko, and L. Maleki, *Phys. Rev. Lett.* **92**, 043903 (2004).
- [5] T. Aoki, B. Dayan, E. Wilcut, W. P. Bowen, A. S. Parkins, T. J. Kippenberg, K. J. Vahala, and H. J. Kimble, *Nature (London)* **443**, 671 (2006).
- [6] Y.-S. Park, A. K. Cook, and H. Wang, *Nano Lett.* **6**, 2075 (2006).
- [7] T. J. Kippenberg, H. Rokhsari, T. Carmon, A. Scherer, and K. J. Vahala, *Phys. Rev. Lett.* **95**, 033901 (2005).
- [8] Y. S. Park and H. Wang, *Nature Phys.* **5**, 489 (2009).
- [9] A. H. Safavi-Naeini, T. P. Mayer Alegre, J. Chan, M. Eichenfield, M. Winger, Q. Lin, J. T. Hill, D. E. Chang, and O. Painter, *Nature* **472**, 69 (2011).
- [10] J. S. Foresi, P. R. Villeneuve, J. Ferrera, E. R. Thoen, G. Steinmeyer, S. Fan, J. D. Joannopoulos, L. C. Kimerling, H. I. Smith, and E. P. Ippen, *Nature* **390**, 143 (1997).
- [11] H. Rokhsari and K. J. Vahala, *Phys. Rev. Lett.* **92**, 253905 (2004).
- [12] V. Sandoghdar, F. Treussart, J. Hare, V. Lefevre-Seguin, J.-M. Raimond, and S. Haroche, *Phys. Rev. A* **54**, R1777 (1996).
- [13] G. S. Solomon, M. Pelton, and Y. Yamamoto, *Phys. Rev. Lett.* **86**, 3903 (2001).
- [14] L. Yang, D. K. Armani, and K. J. Vahala, *Appl. Phys. Lett.* **83**, 825 (2003).
- [15] Y.-F. Xiao, C.-H. Dong, C.-L. Zou, Z.-F. Han, L. Yang, and G.-C. Guo, *Opt. Lett.* **34**, 509 (2009).
- [16] F. Vollmer, D. Braun, A. Libchaber, M. Khoshhima, I. Teraoka, and S. Arnold, *Appl. Phys. Lett.* **80**, 4057 (2002).
- [17] I. M. White, H. Oveys, and X. Fan, *Opt. Lett.* **31**, 1319 (2006).
- [18] F. Vollmer, S. Arnold, and D. Keng, *Proc. Natl. Acad. Sci. U.S.A.* **105**, 20701 (2008).
- [19] J. Zhu, S. K. Ozdemir, Y.-F. Xiao, L. Li, L. He, D.-R. Chen, and L. Yang, *Nature Photon.* **4**, 46 (2010).
- [20] T. Lu, H. Lee, T. Chen, S. Herchak, J.-H. Kim, S. E. Fraser, R. C. Flagan, and K. Vahala, *Proc. Natl. Acad. Sci.* **10**, 1073 (2011).
- [21] Y.-F. Xiao, C.-L. Zou, B.-B. Li, Y. Li, C.-H. Dong, Z.-F. Han, and Q. Gong, *Phys. Rev. Lett.* **105**, 153902 (2010).
- [22] V. B. Braginsky, M. L. Gorodetsky, and V. S. Ilchenko, *Phys. Lett. A* **137**, 393 (1989).
- [23] J. C. Knight, G. Cheung, F. Jacques, and T. A. Birks, *Opt. Lett.* **22**, 1129 (1997).
- [24] M. Cai, O. Painter, and K. J. Vahala, *Phys. Rev. Lett.* **85**, 74 (2000).
- [25] V. S. Ilchenko, X. S. Yao, and L. Maleki, *Opt. Lett.* **24**, 723 (1999).
- [26] S.-B. Lee, J. Yang, S. Moon, J.-H. Lee, and K. An, *Appl. Phys. Lett.* **90**, 041106 (2007).
- [27] J. Yang, S.-B. Lee, S. Moon, S.-Y. Lee, S.W. Kim, T. T. A. Dao, J.-H. Lee, and K. An, *Phys. Rev. Lett.* **104**, 243601 (2010).
- [28] J. U. Nöckel and A. D. Stone, *Nature* **385**, 45 (1997).
- [29] Y.-S. Park and H. Wang, *Opt. Express* **15**, 16471 (2007).
- [30] U. Fano, *Phys. Rev.* **124**, 1866 (1961).
- [31] Y.-F. Xiao *et al.*, unpublished.
- [32] C. Gmachl *et al.*, *Science* **280**, 1556 (1998).
- [33] M. Hentschel and K. Richter, *Phys. Rev. E* **66**, 056207 (2002).
- [34] V. I. Arnol'd, *Russ. Math. Surv.* **18**, 9 (1963).
- [35] S.-Y. Lee and K. An, *Phys. Rev. A* **83**, 023827 (2011).
- [36] C. L. Zou, F. W. Sun, C. H. Dong, X. W. Wu, J. M. Cui, Y. Yang, G. C. Guo, Z. F. Han, <http://arxiv.org/abs/0908.3531>.
- [37] X. F. Jiang, Y. F. Xiao, C.-L. Zou, L. He, C.-H. Dong, B.-B. Li, Y. Li, F.-W. Sun, L. Yang, and Q. Gong, *Adv. Mat.* **24**, OP260 (2012).
- [38] M. Hentschel, H. Schomerus, and R. Schubert, *Europhys. Lett.* **62**, 636 (2003).
- [39] As the regular mode lies on an invariant torus behaving much like whispering gallery mode, we use WGM to represent it.
- [40] A. Bäcker, R. Ketzmerick, S. Löck, and L. Schilling, *Phys. Rev. Lett.* **100**, 104101 (2002).
- [41] C.W. Gardiner and P. Zoller, *Quantum Noise*, 3rd ed. (Springer, Berlin, 2004).
- [42] H. Schomerus and M. Hentschel, *Phys. Rev. Lett.* **96**, 243903 (2006).
- [43] J. Yang, S.-B. Lee, S. Moon, S.-Y. Lee, S. W. Kim, and K. An, *Opt. Express* **18**, 26141 (2010).
- [44] T. Geisel, G. Radons, and J. Rubner *Phys. Rev. Lett.* **57**, 2883 (1986).
- [45] I. I. Rypina, M. G. Brown, F. J. Beron-Vera, H. Kocak, M. J. Olascoaga, and I. A. Udovydchenkov *Phys. Rev. Lett.* **98**, 104102 (2007).
- [46] J.-B. Shim, S.-B. Lee, S. W. Kim, S.-Y. Lee, J. Yang, S. Moon, J.-H. Lee, and K. An, *Phys. Rev. Lett.* **100**, 174102 (2008).
- [47] Q. Song, L. Ge, B. Redding, and H. Cao *Phys. Rev. Lett.* **108**, 243902 (2012).